Progress In Electromagnetics Research, Vol. 172, 51–60, 2021

Wideband High-Reflection Chiral Dielectric Metasurface

Zhipeng Hu[1], Nan He[1, 2], Yuwei Sun[1], Yi Jin[1, *], and Sailing He[1, 2, 3, *]

Abstract—Compared to natural materials, artificial subwavelength structures can enhance chiroptical effects in a stronger way, and the requirement of low material loss and wideband operation is desired in many situations. Here, we propose an all-dielectric chiral metasurface as a periodic array of centrosymmetric staggered silicon cuboid pairs to achieve strong circular dichroism in a wide band. As a demonstration, the designed chiral metasurface may strongly reflect the chosen circularly polarized light with the spin preserved in the operating wavelength range of $1.51 \sim 1.60\,\mu\mathrm{m}$ while highly transmit (with an efficiency greater than 95%) the opposite circularly polarized light with the spin flipped. Then, two application cases are given for the designed chiral metasurface. A flat chiral meta-lens is constructed to produce wideband focusing in the transmission/reflection side while the disturbing from the opposite circular polarization is well blocked by high reflection/transmission. A chiral Fabry-Perot cavity is also constructed, which has an extremely high quality factor (2.1E4). The proposed method provides an efficient way to produce strong chiroptical effects and has a promising potential for various applications such as signal processing, sensing, radiation and detection.

1. INTRODUCTION

Chiroptical effects widely exist in various natural substances, such as gas molecules, organic matters, crystals and so on. The optical activity and circular dichroism of a chiral material are the two main mechanisms used to distinguish their enantiomers [1–4]. However, the direct interaction between the chiral material molecules/elements and light beam is quite weak due to thescale mismatch. Thus, one needs to increase the optical path and collision times to amplify the interaction and response signal. This would lead to an increase in the volume of the system. With the development of metasurface technology, ultra-thin metal chiral structures have been proposed [5–8], and some special designs can enhance the chiroptical response by multiple orders of magnitude, such as three-dimensional gold helix [9–11], two-dimensional fish-scale structure [12–14], and L-shaped gold nanoantennas [15–18]. However, due to metal absorption loss, the efficiency is limited. In recent years, lossless dielectric chiral metasurfaces have attracted much attention and utilized to achieve low loss, high refractive index, large field enhancement, excitation of high-order Mie resonance modes, or more efficient optical manipulation with higher degrees of freedom, and many structures with outstanding performance have been designed [19–27]. These lossless ultra-thin chiral metasurface structures were small in size, high in efficiency, and rich in functions, and can be used for detection of chiral substances, as well as metalenses toreplace the traditional large-volume optical components, such as lenses, polarizers, quarter glass slides, etc. However, most of these reported designs only have narrow-band optical responses, and can only be used for a single wavelength or narrowband range, which severely restricts the applications of chiral metasurfaces.

Received 19 December 2021, Accepted 30 December 2021, Scheduled 31 December 2021

* Corresponding author: Yi Jin (jinyi_2008@zju.edu.cn), Sailing He (sailing@kth.se).

[1] Center for Optical and Electromagnetic Research, State Key Laboratory for Modern Optical Instrumentation, Zhejiang University, Hangzhou 310058, China. [2] Shanghai Institute for Advanced Study, Zhejiang University,Shanghai 200000, China. [3] Department of Electromagnetic Engineering, School of Electrical Engineering, Royal Institute of Technology (KTH), Stockholm S-100 44, Sweden.

In this article, a lossless dielectric chiral metasurface working in a broadband (in the near-infrared region) is designed. Based on the CP transmission/reflection characteristics of the proposed structure, we demonstrate a chiral metalens with one of the CP light beams is transmissively/reflectively focused, while the other is blocked (i.e., highly reflected/transmitted). Furthermore, a chiral Fabry-Perot (FP) cavity is designed. The designed FP cavity has an extremely high quality factor as large as 2.1E4 and also has an interesting property of spin-preserving filter for chosen CP light. Meanwhile, the chiral FP cavity resonance can form a spiral standing wave (without resonant nodes) that is nearly uniform, which is a very prominent property [28]. The novel chiral optical devices may have future applications in collection, detection, enhancement and filteringfor chiral signals.

2. DESIGNING A WIDE-BAND HIGH-REFLECTION CHIRAL DIELECTRIC METASURFACE

The designed chiral metasurface is a periodic array consisting of centrosymmetric staggered silicon cuboid pairs deposited on a silicon oxide (SiO_2) thin film suspended in the free space. The width, length and height of each cuboid are w, l and h, respectively, the period is p, and the thickness of the SiO_2 thin film is t. In the numerical investigation (via Lumerical FDTD) for the behavior of the metasurface, a circularly polarized illuminating light is realized by superposing two linearly orthogonally polarized sources between which there is $\pm\pi/2$ relative phase retardance. As illustrated by the inset of Fig. 1, for an observer viewing along the propagating direction of an incident or scattered light, it is defined that the light is left-handed circularly polarized (LCP) if the electric field spins clockwise, and right-handed circularly polarized (RCP) if the electric field spins anticlockwise. In the following, an incident light normally impinges on the metasurface by default.

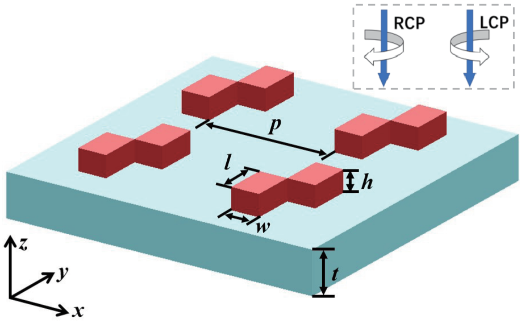

Figure 1. Configuration of the proposed chiral metasurface. The metasurface, consisting of a periodical array of centrosymmetric staggered silicon cuboid pairs, is put on a sustained SiO_2 film. The inset illustrates the definition of RCP and LCP waves.

When the geometry parameters of the metasurface in Fig. 1(a) are set as $h = 680\,\text{nm}$, $l = 412\,\text{nm}$, $w = 273\,\text{nm}$, $p = 1272\,\text{nm}$, and $t = 1000\,\text{nm}$, the transmission and reflection property is shown in Fig. 2. In the wavelength range between 1.51 µm and 1.60 µm, the reflection efficiency (R_{RCP}) is larger than 95% under RCP incidence, and the corresponding transmission efficiency (T_{RCP}) is lower than 5% since the material loss is omittable. Oppositely, the reflection efficiency (R_{LCP}) is lower than 5% for LCP incidence while the transmission efficiency (T_{LCP}) is greater than 95%. Especially at wavelength $\lambda = 1585\,\text{nm}$, the RCP incident light is reflected nearly perfectly and the LCP one passes through the metasurface nearly completely. To valuate the circular dichroism (CD) effect of the metasurface, the CD_{T} for the transmission is defined as

$$CD_{\text{T}} = \tan^{-1}\left(\frac{T_{\text{RCP}} - T_{\text{LCP}}}{T_{\text{RCP}} + T_{\text{LCP}}}\right), \tag{1}$$

and CD_{R} for the reflection may also be defined in a similar way [29, 30]. The CD_{R} and CD_{T} spectra are shown in Fig. 2(b) which indicates that the metasurface presents strongly different response to RCP and LCP incidence in a wide bandwidth.

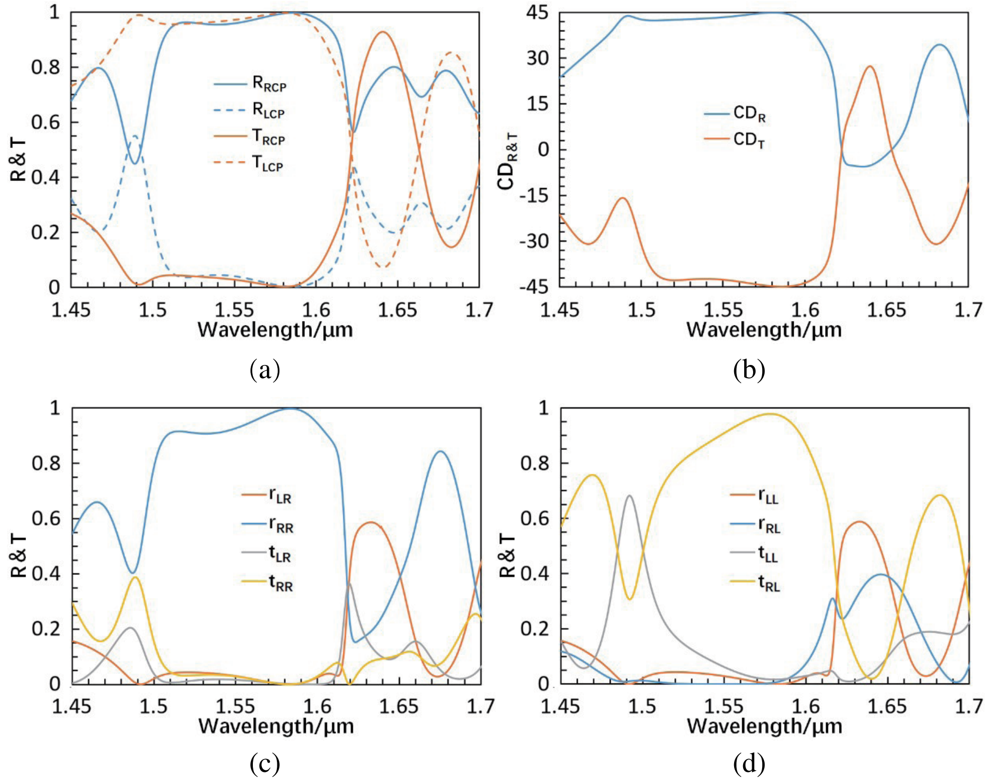

(a) (b) (c) (d)

Figure 2. Reflection and transmission response of the designed metasurface. (a) Polarization-unresolved transmission and reflection efficiencies under different circularly polarized incidences. (b) Transmission and reflection CD spectra. Circular polarization-resolved reflection and transmission efficiencies (c) for RCP incidence and (d) for LCP incidence. The metasurface configuration is shown in Fig. 1, and the corresponding structure parameters are $h = 680\,\text{nm}$, $l = 412\,\text{nm}$, $w = 273\,\text{nm}$, $p = 1272\,\text{nm}$, and $t = 1000\,\text{nm}$.

Then, to disclose the polarization conversion induced by the metasurface, the Jones matrix is adopted to decompose the transmitted and reflected waves into LCP and RCP components [31]. For RCP incidence, the reflected LCP and RCP powers normalized to the incident RCP one is denoted by r_{LR} and r_{RR}, respectively, and the normalized transmitted components denoted by t_{LR} and t_{RR}, respectively. And, r_{LL}, r_{RL}, t_{LL}, and t_{RL} are adopted for LCP incidence. The simulated polarization-resolved reflection and transmission efficiencies are given in Figs. 2(c) and 2(d). One can see that the designed metasurface exhibits strong chiroptical response. In the wavelength range between 1.51 μm and 1.60 μm, r_{RR} is large and r_{LR} is little when RCP incident wave is strongly reflected, which indicates that the original circular polarization can be remained in a large degree during reflection. Especially at $\lambda = 1585\,\text{nm}$, the reflected light is almost RCP. In the same wavelength range, the metasurface weakly blocks the LCP incidence, but strongly converses the original circular polarization during transmission since t_{RL} is large and t_{LL} is omittable. At $\lambda = 1585\,\text{nm}$, the transmitted light is almost RCP. In all, the designed metasurface possesses maximal chiroptical response, and it can convert an incident wave of arbitrary polarization into a pure RCP wave, that is, both the reflected and transmitted waves are RCP.

A high-contrast grating (HCG), whose period is close to the working wavelength, can support wideband high reflection [32]. Common HCGs are a periodic array of long dielectric bars or symmetric dielectric particles. Here, with the introduction of planar-type chiral dielectric units, the designed metasurface behaves in strong contrast at different circular-polarization incidences, that is, it acts as a mirror for RCP incidence and as a twisted pipe which weakly obstructs the power flowing of LCP incidence, but flips the circular polarization to RCP polarization. This response difference is embodied by the excited localized field distribution around the metasurface. Fig. 3 shows the electric amplitude distributions along different transverse cross-sections parallel to the xy-plane at several discrete wavelengths in the interesting wavelength range between 1.51 μm and 1.60 μm. By observing Fig. 3, one can know that strong mutual coupling exists between the electric fields around the neighboring cuboids in each unit, and the electric pattern does not change strongly in the investigated wavelength range for a fixed circularly polarized incidence. However, the electric patterns for RCP incidence are obviously different from those for LCP incidence. The electric field induced by LCP incidence is mainly dispersed in the air near the periphery of each cuboid pair as shown in Fig. 3(b). At RCP incidence, as shown by the first and second rows in Fig. 3(a), there exists strong electric field inside each silicon cuboid pair which may be even stronger than that in the air near the cuboid periphery, and as shown by the third row in Fig. 3(a), although the external electric field is obviously stronger than the internal electric filed, the position possessing strong electric field at RCP incidence is different from that at LCP incidence.

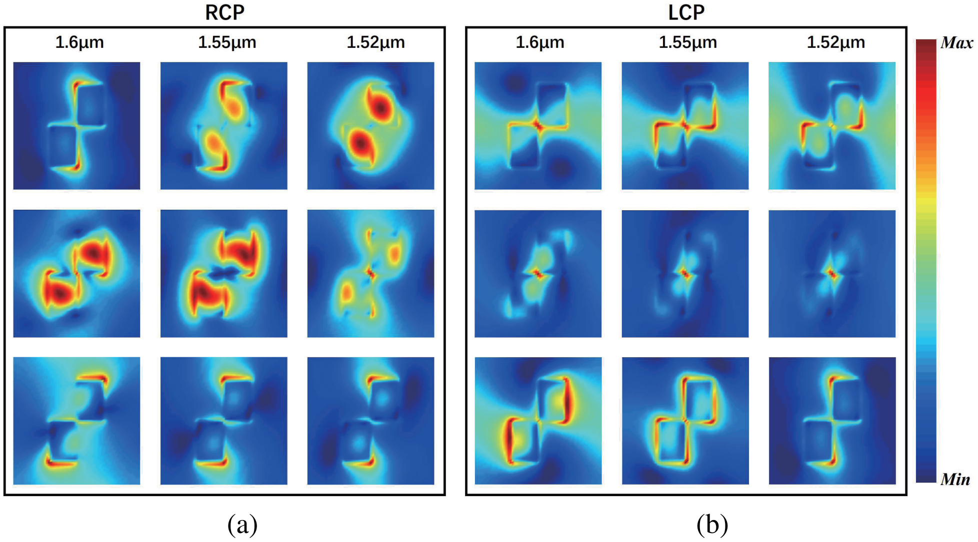

Figure 3. Electric amplitude distributions around the designed chiral metasurface. (a) is for RCP incidence and (b) for LCP incidence. The electric amplitude is normalized by that of the incident wave. From the first row to the third row in each figure, the substrate-Si interface, the middle transverse cross section of the Si metasurface, and the air-Si interface are taken as the observation plane, respectively. And, the first column to the third column in each figure are taken at wavelength $\lambda = 1.6$ μm, 1.55 μm, and 1.52 μm, respectively.

3. CONSTRUCTING A CHIRAL FLAT META-LENS BASED ON A GRADIENT CHIRAL METASURFACE

Based on the polarization-selective transmission and reflection function, here the above designed chiral metasurface is used to construct a polarization-selective flat focusing meta-lens by appropriately adjusting each unit cell as a lens element. Its characteristic is that only a certain circularly polarized beam is allowed to get transmitted or reflected to focus at one side. Therefore, the chiral meta-lens will achieve a focused beam of a highly pure circular polarization. This is different from classical lenses and flat meta-lenses. In common meta-lenses based on the Pancharatnam-Berry (PB) phase [19], one of RCP and LCP incident beams is focused and the other one is diverged, but both are highly transmitted or reflected simultaneously so that they may disturb each other strongly.

The designing method of the current chiral meta-lens is the same as that of common PB-type meta-lenses. For simplicity, investigation is made only for focusing an RCP incident beam, and similar deal can be made for an LCP incident beam. By choosing the geometry type (R or L) of the original chiral metasurface, the chiral meta-lens acts as a concave mirror or a convex lens for the RCP incident beam. Each meta-lens element is rotated in an angle of φ in the following way [19],

$$\varphi(x) = \pm 0.5 k_0 \left(\sqrt{f^2 + x^2} - |f| \right), \tag{2}$$

where x is the position of the meta-lens element relative to the lens center; $k_0 = 2\pi/\lambda$ is the free-space wavevector; f is the focal length of the lens; the "$-$" sign corresponds to a reflective focusing lens (concave mirror) while the "+" sign corresponds to a transmissive focusing lens (convex lens).

Figure 4(a) illustrates the configuration of a cylindrical chiral meta-lens. The original chiral metasurface is R-type, highly reflecting the RCP incident beam as shown in Fig. 2, so that a concave mirror can be constructed. To construct a cylindrical concave mirror, each meta-lens element is rotated according to Eq. (2) where x is the distance between the element and the cylindrical axis along the y direction, and "$-$" is adopted. The constructed concave mirror shown in Fig. 4(a) has a focal length of 40 µm, which is periodic array of finite-width rows consisting of 21 meta-lens elements (10 elements on each side of the central element).

By optimizing the concave mirror for the RCP beamin a broad band of 1.51 ∼ 1.60 µm, we obtain $p_x = 1$ µm and $p_y = 1.272$ µm, and the other geometry parameters of the metasurface are the same

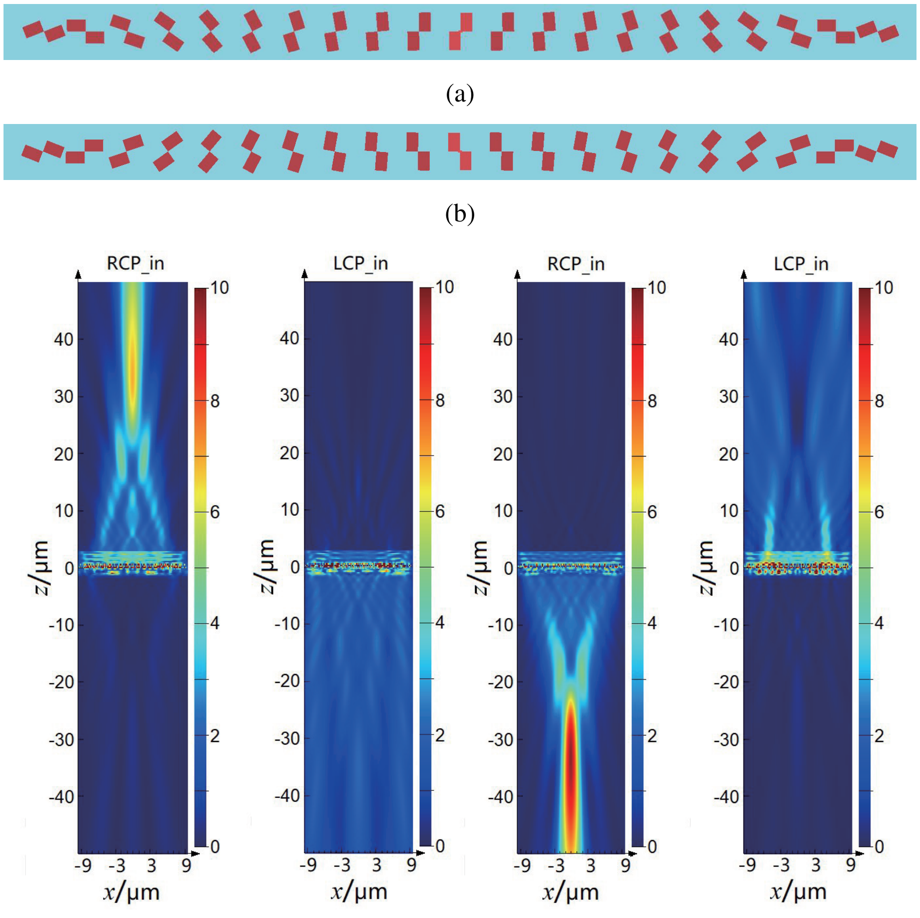

Figure 4. Cylindrical chiral meta-lens. (a) Concave mirror, and (b) convex meta-lens designed to operate for an RCP beam incident upwards. (c) and (d) are electric amplitude distributions when the meta-lens in (a) is illuminated upwards by an RCP beam and an LCP beam, respectively. (e) and (f) are electric amplitude distributions when the meta-lens in (b) is illuminated by an RCP beam and an LCP beam, respectively. The numerical results are shown at the edge wavelength of 1.6 µm and the focusing length is 40 µm. Each electric amplitude distribution is normalized by that of the corresponding incident beam.

as those used in Fig. 2. Fig. 4(c) demonstrates the electric focusing pattern of the RCP beam(at the edge wavelength of 1.60 µm) incident upwards. The RCP beam is strongly reflected and shrinks toward the focusing point. When the incident beam is switched from the RCP state to the LCP state, the corresponding electric distribution around the meta-lens is shown in Fig. 4(d), where one sees that the LCP beam is of high transmission, but cannot be focused at the other side of the meta-lens.

Figure 4(b) illustrates the configuration of another cylindrical chiral metasurface as a convex meta-lens. The original chiral metasurface is L-type, which weakly reflects the RCP incident beam so that a convex meta-lens can be constructed. When $p_x = 1\,\mu\text{m}$ and $p_y = 1.272\,\mu\text{m}$, and the geometry parameters are the same as those used in Fig. 2, Fig. 4(e) demonstrates the electric focusing pattern of the RCP beam incident upwards. The beam is highly transmitted and shrinks toward the focusing point at the bottom side of the meta-lens. When the incident beam is switched from the RCP state to the LCP state, the corresponding electric distribution around the meta-lens is shown in Fig. 4(f). One can see that the LCP beam is highly reflected, but it cannot be focused at the top side of the meta-lens.

To quantitatively evaluate the operation performance of the above two chiral meta-lenses, calculation is made for the reflection efficiencies of the concave mirror in Fig. 4(a) and the transmission efficiencies of the convex lens in Fig. 4(b) illuminated by the RCP and LCP incident beams, and the results are shown in Figs. 5(a) and 5(b), respectively. By observing Fig. 5, one can see that the two meta-lens may sustain good polarization selectivity in a wide band that the RCP beam is focused efficiently while the LC beam is inhibited at the focusing image in a high degree. This kind of magical chiral meta lens may be applied to collect and detect the chiral signals with high signal to noise ratio.

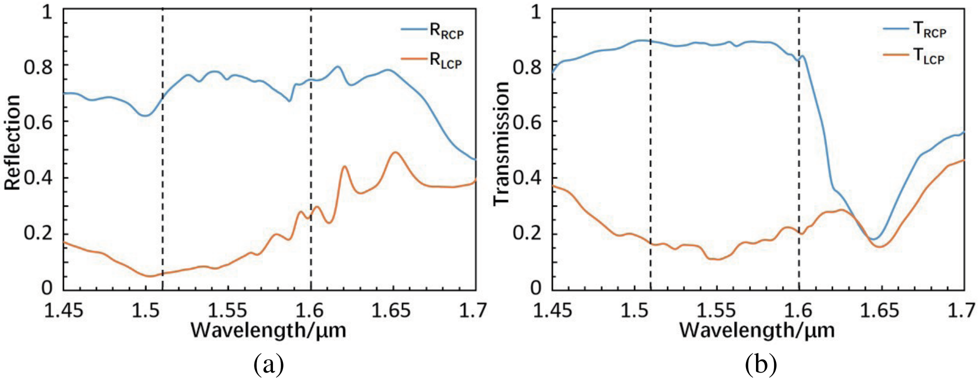

Figure 5. Performance of a chiral meta-lens. Under different circularly polarized incidences, the polarization-unresolved transmission efficiencies of the meta-lens structure in Fig. 4(a) is shown in (a), and the polarization-unresolved reflection efficiencies of the meta-lens structure in Fig. 4(d) are shown in (b).

4. CONSTRUCTING A CHIRAL FP CAVITY BASED ON TWO SYNTHETICS CHIRAL METASURFACES

The above designed chiral dielectric metasurface works as a wide-band chiral mirror for RCP light. Then, one can construct a chiral FP cavity by cascading two chiral mirrors as illustrated by Fig. 6(a). The R-type metasurface with the supporting dielectric film shown in Fig. 1(a) acts as the bottom cavity mirror, and it also acts as the top cavity mirror after being normally flipped. As demonstrated in Fig. 6(a), the separation between the two mirrors is defined as the cavity length of L_c. The wideband operation of the mirrors reduces the precision requirement of the cavity length to form FP resonance.

The resonance mechanism of the chiral FP cavity can be understood in the following way. It is assumed that an RCP light is incident on the bottom metasurface at the beginning. The RCP light is strongly reflected while the circular polarization is maintained. When the reflected RCP light arrives at the top metasurface, this metasurface is also R-type in its view so that it continues to be strongly reflected with the circular polarization maintained. As the RCP light, experiencing strong reflection twice, returns to the bottom metasurface, a closed light path is formed. If the phase retardance along this closed path satisfies the FP resonance condition, a resonant mode is formed. In this FP mode, the main component is RCP, and the LCP component is surely weak since it can leak through the top and bottom metasurfaces well.

Then, the response of the constructed cavity to different light illumination is investigated. The geometry parameters of the metasurfaces forming the cavity are the same as those used in Fig. 2. With $L_c = 1.6\,\mu\text{m}$, the transmission of the chiral FP cavity under different circularly polarized illuminating beams is shown in Fig. 6(b). One can see that for LCP incidence, the polarization-unresolved transmission (i.e., without decomposing the transmitted wave into LCP and RCP components) of the cavity is low in a wide wavelength range around $\lambda = 1585\,\text{nm}$, but there is an obvious near-unity transmission peak at $\lambda = 1585.25\,\text{nm}$. The full width at half maximum of this resonance peak is only 0.075 nm, and the corresponding quality factor is as large as 21000. This means that the FP resonant mode has a rather low leaky rate and can be excited by an LCP light. To observe the polarization-

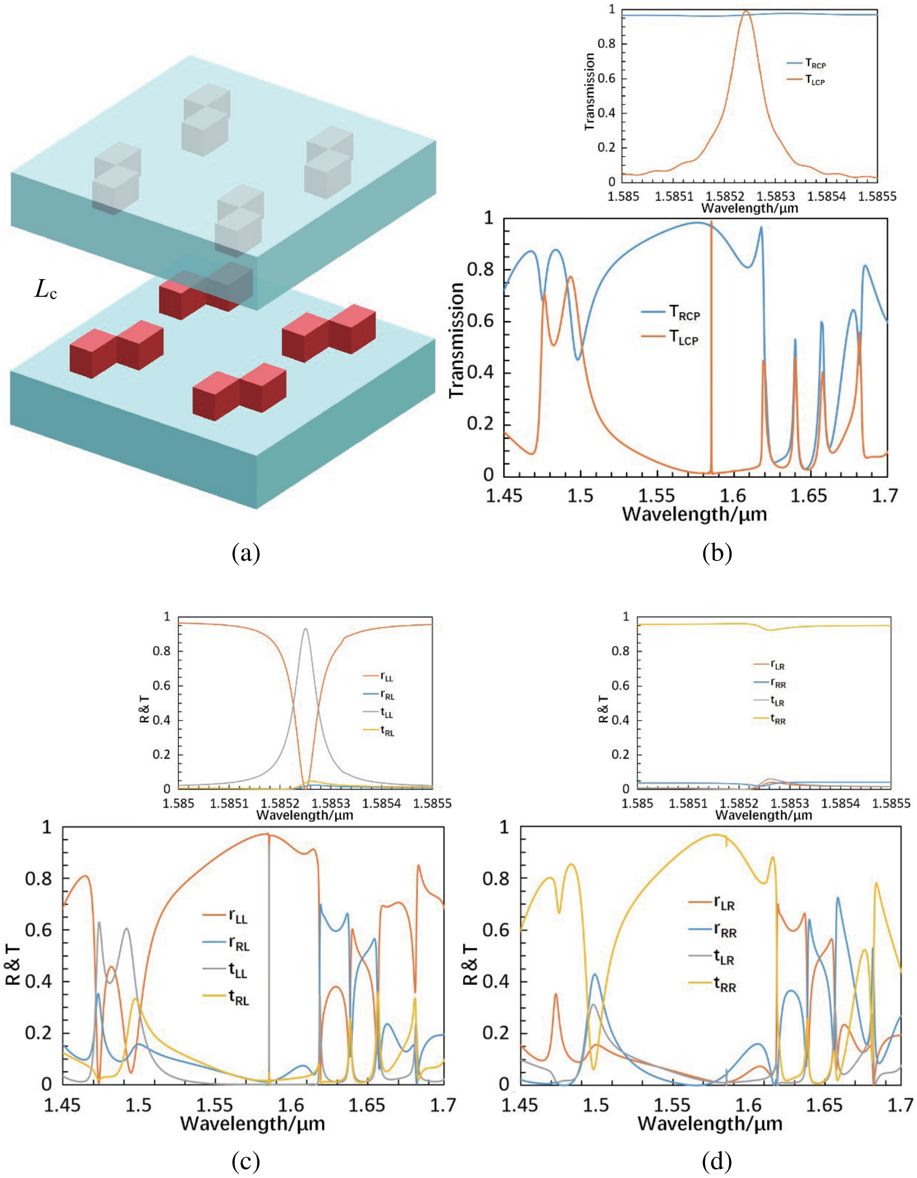

(a) (b)

(c) (d)

Figure 6. Chiral FP cavity. (a) Cavity configuration. (b) Polarization-unresolved transmission. (c) Polarization-resolved transmission and reflection for LCP incidence, and (d) those for RCP incidence. The magnified views around the resonance peak at $\lambda = 1585.25\,\text{nm}$ are also given at the top in (b), (c) and (d).

resolved transmission and reflection for LCP incidence, the transmitted and reflected waves are further decomposed into LCP and RCP components. The decomposition result is shown in Fig. 6(c). One can observe that at the resonant peak of $\lambda = 1585.25\,\text{nm}$, t_{RL} is high up to 95% and t_{RL} is low down to 5%. Near the resonant peak, the main component of the reflected wave is LCP. This indicates that cross polarization in the cavity transmission is weak. Thus, the chiral FP cavity works well as a narrow-band polarization-maintaining filter for LCP incidence.

In contrast, as shown by Fig. 6(b), the transmission keeps high for RCP incidence, and the corresponding transmission curve varies smoothly in the investigated wavelength range around $\lambda = 1585\,\text{nm}$. It means that the RCP light cannot effectively excite the FP resonant mode. The transmitted and reflected waves are also decomposed into LCP and RCP components and the result is shown in Fig. 6(d). The main component of the transmitted wave keeps RCP in the investigated wavelength range. One may also notice the weak narrow dip on the transmission curve of r_{RR} and the weak narrow peak on the reflection curve of r_{LR}. This is because the RCP incidence may excite the FP resonance through cross polarization, but nevertheless this excitation is rather weak.

To investigate the pattern feature of the FP resonant mode, the electric intensity distributions on several observation planes at the resonant peak under LCP incidence are calculated and shown in Fig. 7. Since the top and bottom metasurfaces as mirrors are periodic, the electric distributions present obvious periodic variation. Because the FP is strongly excited, the electric field inside the cavity is very strong, and the intensity can be enhanced in more than 3000 times compared to the incident one. The electric field is the strongest around the top and bottom metasurfaces. At last, one should notice that the electric field inside the air region sandwiched between the top and bottom metasurfaces is nearly homogeneous. This is the representative characteristic of a chiral FP resonant mode [28].

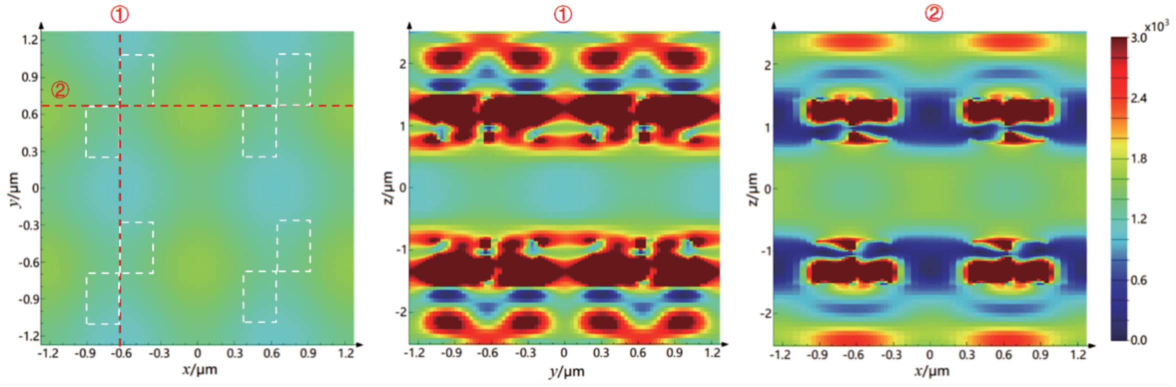

(a) (b) (c)

Figure 7. Mode field distribution. The corresponding electric field distributions at different cross-sections of the chiral FP cavity: (a) is at the center of the cavity in the xy-plane; (b) and (c) are on the corresponding vertical cross sections as referred by the dotted lines ① and ② in (a), respectively.

5. CONCLUSIONS

In this paper, we have proposed an all-dielectric planar-type chiral metasurface behaving like a special HCG to support loss-less wideband chiroptical operation. This demonstrated in the wide wavelength range of $1.51 \sim 1.60\,\mu\text{m}$ a metasurface that reflects with a high efficiency over 95% for a chosen circular polarization and transmits highly for the opposite circularly polarized light with the spin flipped. Two devices have also been constructed and investigated as application cases. The wideband flat chiral meta-lens has its particular advantage, that is, only the chosen circular polarization among the arbitrarily incident light is focused in the transmission/reflection side while the perturbation from the opposite circular polarization is well blocked. In addition, the wideband chiral metasurface is helpful in constructing a unique chiral FP cavity, and the constructed cavity has a large quality factor of 2.1E4. In all, the suggested method provides an efficient way to manipulate chiroptical operation and opens the way to various special chiral devices.

ACKNOWLEDGMENT

This work has been partially supported by the National Natural Science Foundation of China (61875174, 91833303, and 11621101), National Key Research and Development Program of China (2017YFA0205700), the Fundamental Research Funds for the Central UniversitiesandSpecial Development Fund of Shanghai Zhangjiang Science City.

REFERENCES

1. Ben-Moshe, A., B. M. Maoz, A. O. Govorov, and G. Markovich, "Chirality and chiroptical effects in inorganic nanocrystal systems with plasmon and exciton resonances," *Chemical Society Reviews*, Vol. 42, No. 16, 7028–7041, 2013.
2. Collins, J. T., C. Kuppe, D. C. Hooper, C. Sibilia, M. Centini, and V. K. Valev, "Chirality and chiroptical effects in metal nanostructures: Fundamentals and current trends," *Advanced Optical Materials*, Vol. 5, No. 16, 1700182, 2017.
3. Valev, V. K., J. J. Baumberg, C. Sibilia, and T. Verbiest, "Chirality and chiroptical effects in plasmonic nanostructures: Fundamentals, recent progress, and outlook," *Advanced Materials*, Vol. 25, No. 18, 2517–2534, 2013.
4. Tang, Y. Q. and A. E. Cohen, "Optical chirality and its interaction with matter," *Physical Review Letters*, Vol. 104, No. 16, 163901, 2010.
5. Zhao, Y., A. N. Askarpour, L. Sun, J. Shi, X. Li, and A. Alù, "Chirality detection of enantiomers using twisted optical metamaterials," *Nature Communications*, Vol. 8, No. 1, 14180–14180, 2017.
6. Khanikaev, A. B., N. Arju, Z. Fan, D. Purtseladze, F. Lu, J. Lee, P. Sarriugarte, M. Schnell, R. Hillenbrand, and M. A. Belkin, "Experimental demonstration of the microscopic origin of circular dichroism in two-dimensional metamaterials," *Nature Communications*, Vol. 7, No. 1, 12045–12045, 2016.
7. Poulikakos, L. V., P. Thureja, A. Stollmann, E. D. Leo, and D. J. Norris, "Chiral light design and detection inspired by optical antenna theory," *Nano Letters*, Vol. 18, No. 8, 4633–4640, 2018.
8. Lin, C. Y., C. C. Liu, Y. Y. Chen, K. Y. Chiu, J. D. Wu, B. L. Lin, H. W. Chang, Y. F. Chen, S. H. Chang, and Y. C. Chang, "Molecular chirality detection with periodic arrays of three-dimensional twisted metamaterials," *ACS Applied Materials & Interfaces*, Vol. 13, No. 1, 1152–1157, 2021.
9. Gansel, J. K., M. Thiel, M. S. Rill, M. Decker, K. Bade, V. Saile, G. V. Freymann, S. Linden, and M. Wegener, "Gold helix photonic metamaterial as broadband circular polarizer," *Science*, Vol. 325, No. 5947, 1513–1515, 2009.
10. Esposito, M., V. Tasco, M. Cuscunà, F. Todisco, A. Benedetti, I. Tarantini, M. D. Giorgi, D. Sanvitto, and A. Passaseo, "Nanoscale 3D chiral plasmonic helices with circular dichroism at visible frequencies," *ACS Photonics*, Vol. 2, No. 1, 105–114, 2015.
11. Tseng, M. L., Z. H. Lin, H. Y. Kuo, T. T. Huang, Y. T. Huang, T. L. Chung, C. H. Chu, J. S. Huang, and D. P. Tsai, "Stress-induced 3D chiral fractal metasurface for enhanced and stabilized broadband near-field optical chirality," *Advanced Optical Materials*, Vol. 7, No. 15, 1900617, 2019.
12. Fedotov, V. A., P. L. Mladyonov, S. L. Prosvirnin, A. V. Rogacheva, Y. Chen, and N. I. Zheludev, "Asymmetric propagation of electromagnetic waves through a planar chiral structure," *Physical Review Letters*, Vol. 97, No. 16, 167401–167401, 2006.
13. Fedotov, V. A., A. S. Schwanecke, N. I. Zheludev, V. V. Khardikov, and S. L. Prosvirnin, "Asymmetric transmission of light and enantiomerically sensitive plasmon resonance in planar chiral nanostructures," *Nano Letters*, Vol. 7, No. 7, 1996–1999, 2007.
14. Schwanecke, A. S., V. A. Fedotov, V. V. Khardikov, S. L. Prosvirnin, Y. Chen, and N. I. Zheludev, "Nanostructured metal film with asymmetric optical transmission," *Nano Letters*, Vol. 8, No. 9, 2940–2943, 2008.
15. Najafabadi, A. F. and T. Pakizeh, "Optical absorbing origin of chiroptical activity in planar plasmonic metasurfaces," *Scientific Reports*, Vol. 7, No. 1, 10251–10251, 2017.

16. Ye, W., X. Yuan, C. Guo, J. Zhang, and Z. Shuang, "Large chiroptical effects in planar chiral metamaterials," *Physical Review Applied*, Vol. 7, No. 5, 54003, 2017.
17. Ullah, H., A. Abudukelimu, Y. Qu, Y. Bai, T. Aba, and Z. Zhang, "Giant circular dichroism of chiral l-shaped nanostructure coupled with achiral nanorod: Anomalous behavior of multipolar and dipolar resonant modes," *Nanotechnology*, Vol. 31, No. 27, 275205, 2020.
18. Kong, X. T., L. K. Khorashad, Z. Wang, and A. O. Govorov, "Photothermal circular dichroism induced by plasmon resonances in chiral metamaterial absorbers and bolometers," *Nano Letters*, Vol. 18, No. 3, 2001–2008, 2018.
19. Chen, X., L. Huang, H. Mühlenbernd, G. Li, B. Bai, Q. Tan, G. Jin, C. W. Qiu, S. Zhang, and T. Zentgraf, "Dual-polarity plasmonic metalens for visible light," *Nature Communications*, Vol. 3, No. 1, 1198–1198, 2012.
20. Ma, Z., Y. Li, L. Yang, Y. Gong, and M. Hong, "All-dielectric planar chiral metasurface with gradient geometric phase," *Optics Express*, Vol. 26, No. 5, 6067–6078, 2018.
21. Solomon, M. L., A. A. E. Saleh, L. V. Poulikakos, J. M. Abendroth, and J. A. Dionne, "Nanophotonic platforms for chiral sensing and separation," *Accounts of Chemical Research*, Vol. 53, No. 3, 588–598, 2020.
22. Rana, A. S., I. Kim, M. A. Ansari, M. S. Anwar, and J. Rho, "Planar achiral metasurfaces-induced anomalous chiroptical effect of optical spin isolation," *ACS Applied Materials & Interfaces*, Vol. 12, No. 43, 48899–48909, 2020.
23. Semnani, B., J. Flannery, R. A. Maruf, and M. Bajcsy, "Spin-preserving chiral photonic crystal mirror," *Light-Science & Applications*, Vol. 9, No. 1, 23–23, 2020.
24. Chen, C., S. Gao, W. Song, H. Li, and T. Li, "Metasurfaces with planar chiral meta-atoms for spin light manipulation," *Nano Letters*, Vol. 21, No. 4, 1815–1821, 2021.
25. Wang, S., Z. L. Deng, Y. Wang, Q. Zhou, X. Wang, Y. Cao, B. O. Guan, S. Xiao, and X. Li, "Arbitrary polarization conversion dichroism metasurfaces for all-in-one full poincaré sphere polarizers," *Light-Science & Applications*, Vol. 10, No. 1, 24–24, 2021.
26. Hu, J. P., C. Zhang, Y. G. Dong, A. J. Zeng, and C. H. Wang, "High efficiency all-dielectric pixelated metasurface for near-infrared full-stokes polarization detection," *Photonics Research*, Vol. 9, No. 4, 4000583, 2021.
27. Li, J., J. T. Li, C. L. Zheng, Y. Yang, Z. Yue, X. R. Hao, H. L. Zhao, F. Y. Li, T. T. Tang, L. Wu, J. N. Li, Y. T. Zhang, and J. Q. Yao,"Lossless dielectric metasurface with giant intrinsic chirality for terahertz wave," *Opt. Express*, Vol. 29, 28329–28337, 2021.
28. Plum, E. and N. I. Zheludev, "Chiral mirrors," *Applied Physics Letters*, Vol. 106, No. 22, 775–388, 2015.
29. Solomon, M. L., A. A. E. Saleh, L. V. Poulikakos, J. M. Abendroth, and J. A. Dionne, "Nanophotonic platforms for chiral sensing and separation," *Accounts of Chemical Research*, Vol. 53, No. 3, 588–598, 2020.
30. Bochenkov, V. E. and T. I. Shabatina, "Chiral plasmonic biosensors," *Biosensors*, Vol. 8, No. 4, 120, 2018.
31. Collett, A. E., *Field Guide to Polarization*, SPIE Press, Bellingham, WA, 2005.
32. Karagodsky, V., F. G. Sedgwick, and C. J. Chang-Hasnain, "Theoretical analysis of subwavelength high contrast grating reflectors," *Optics Express*, Vol. 18, No. 16, 16973–16988, 2010.